Magnetoexciton limit of quantum Hall breakdown in graphene

A. Schmitt,[1,*] M. Rosticher,[1] T. Taniguchi,[2] K. Watanabe,[2] J. M. Berroir,[1] G. Ménard,[1] C. Voisin,[1] G. Fève,[1] M. O. Goerbig,[3] B. Plaçais,[1,†] and E. Baudin[1,‡]

[1]*Laboratoire de Physique de l'Ecole normale supérieure, ENS, Université PSL, CNRS, Sorbonne Université, Université de Paris, 24 rue Lhomond, 75005 Paris, France*

[2]*Advanced Materials Laboratory, National Institute for Materials Science, Tsukuba, Ibaraki 305-0047, Japan*

[3]*Laboratoire de Physique des Solides, CNRS UMR 8502, Univ. Paris-Sud, Université Paris-Saclay, F-91405 Orsay Cedex, France*

(Received 10 March 2023; revised 13 July 2023; accepted 1 August 2023; published 31 August 2023)

One of the intrinsic drift velocity limits of the quantum Hall effect is the collective magnetoexciton (ME) instability. It has been demonstrated in bilayer graphene (BLG) using noise measurements [W. Yang *et al.*, Phys. Rev. Lett. **121**, 136804 (2018)]. We reproduce this experiment in monolayer graphene (MLG), and show that the same mechanism carries a direct relativistic signature on the breakdown velocity. Based on theoretical calculations of MLG- and BLG-ME spectra, we show that Doppler-induced instabilities manifest for a ME phase velocity determined by a universal value of the ME conductivity, set by the Hall conductance.

DOI: 10.1103/PhysRevB.108.085438

I. INTRODUCTION

Low-bias quantum Hall (QH) transport is notoriously described in terms of single-electron physics, as exemplified by the edge-channel conductance quantization used in metrology [1–3]. The situation differs at large bias as electrons may couple to the collective particle-hole excitation spectrum (PHES) [4], described by a dispersion relation $\omega(q)$: it includes in the integer QH case both magnetoplasmon (MP) and magnetoexciton (ME) branches [5], and, in the fractional QH case, a magnetoroton (MR) branch [6,7]. High-bias transport also differs in the electric field and current distributions. In a transistor or a Hall bar geometry (length L, width W), the nondissipative Hall current penetrates the Landau insulating bulk so that source and drain get connected via open ballistic orbits (drift velocity $v_x = E_y/B$) [8,9]. The high-bias conductance G_H and Hall conductivity $\sigma_{xy} = G_H = I_x/V_y = \nu G_K$ are still set by the conductance quantum $G_K = e^2/h$ and the filling factor $\nu = nh/eB$ at a carrier density n. This ballistic transport is ultimately limited by the quantum Hall effect breakdown (QHEBD), a bulk effect occurring at a critical voltage V_{bd} (or field $E_{bd} = V_{bd}/W$, or velocity $v_{bd} = E_{bd}/B$), which is signaled by the onset of a longitudinal voltage $V_x = LE_x$ associated with a bulk backscattering current and its associated shot noise S_I. The most frequently considered QHEBD mechanism is inter-Landau-level tunneling (ILLT), a single-particle effect that sets in when the wave functions of neighboring Landau-levels (LL) overlap in the tilted potential under applied bias [10]. In the case of a massive 2D electron gas called 2DEG, ILLT has a critical Zener field $E_Z \sim \hbar\omega_c/eR_c$, where $\omega_c = eB/m^*$ and $R_c \sim \sqrt{N}l_B$ are the cyclotron angular frequency and radius, m^* is the effective mass, N the number of occupied LLs, and $l_B = \sqrt{\hbar/eB}$ the magnetic length [10]. ILLT gives rise to quite large velocities $v_Z \sim \hbar/m^*R_c$ ($\sim 2.10^5$ m.s^{-1} for $N = 1$ at $10\,T$ with $m^* \simeq 0.06\,m_0$ for GaAs-based 2DEGs). Hall bar experiments indicate premature breakdowns with $v_{bd} \lesssim v_Z/10$ in both 2DEGs and graphene (see [11] and references therein). Several mechanisms have been considered to explain this discrepancy, such as the phonon- or impurity-assisted ILLT [10,12]. Such extrinsic mechanisms are actually needed to overcome the momentum-conservation protection of ILLT, which stems from the $2k_F$ momentum mismatch between neighboring LL wave functions [13], where k_F is the Fermi momentum. However, larger velocities $v_{bd} \sim v_Z/2$ have been reported in quantum Hall constrictions [14,15], thanks to a more uniform electrostatic landscape in the absence of invasive voltage probes. These experiments challenge the single-particle ILLT interpretation, and motivate alternative explanations in terms of collective excitations, such as the ME-instability scenario proposed in Ref. [11].

QHEBD was recently investigated in bilayer graphene (BLG) transistors using shot noise as a probe of ballistic transport breakdown [11]. Interestingly, doped BLG emulates a massive 2DEG with $m^* \simeq 0.03\,m_0$. In the two-terminal transistor geometry, the breakdown was monitored by the sharp onset of the microwave shot-noise current $I_N = S_I/2e$ above the noiseless ballistic Hall background. Breakdown noise is characterized by a large differential noise conductance $G_N = \partial I_N/\partial V$ exceeding the DC Hall conductance G_H. These large values signal a strongly superpoissonian backscattering shot noise which has been interpreted in Ref. [11] as a signature of a collective magnetoexciton (ME) instability, calling for a kinematic origin of breakdown. The $\omega(q \sim k_F)$ sector of the 2DEG-PHES, which is relevant for breakdown in 2DEGs, being essentially interaction independent (see [5] and discussion below), the ME-instability velocity $v_{ME}^{BLG} \sim \hbar/m^*R_c$ turns out

*aurelien.schmitt@phys.ens.fr
†bernard.placais@phys.ens.fr
‡emmanuel.baudin@phys.ens.fr

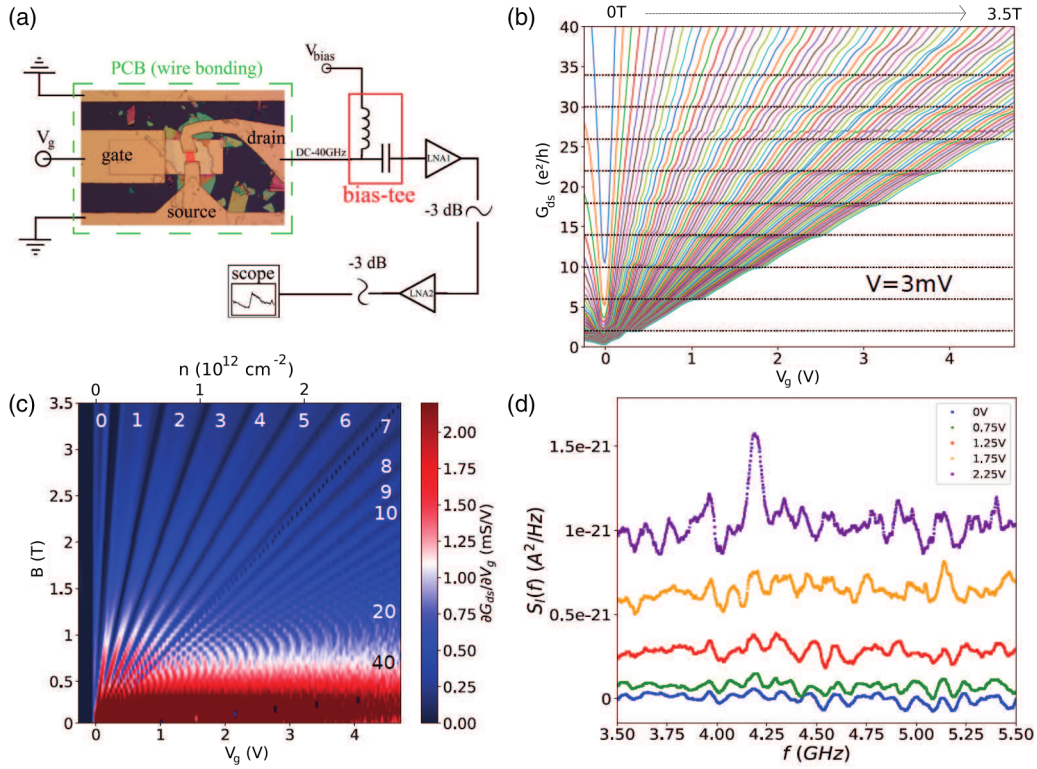

FIG. 1. Low-bias magnetotransport and noise in high-mobility bottom-gated hBN-encapsulated graphene sample AuS2 measured at $T = 4$ K. Sample dimensions are $L \times W \times t_{hBN} = 16 \times 10.6 \times 0.032$ µm. The contact resistance and mobility are $R_c = 36$ Ohms and $\mu = 32$ m^2/Vs. (a) sketch of the measuring setup. (b) Low-bias ($V = 3$ mV) conductance quantization steps in units of e^2/h, obeying the MLG quantization sequence $\nu = 2(2N + 1)$ for the filling factor ν as function of the Landau index N. (c) Fan chart of the zero-bias differential conductance $\partial G_{ds}/\partial V_g$ showing a series of Landau levels. In (b) and (c), the feature inside the N=7 Landau level (at $G \simeq 27\, e^2/h$) is a measurement artifact. (d) Typical shot-noise spectra in increasing bias at $n = 2.10^{12}$ cm^{-2}, $B = 0.5$ T.

to be similar to the interaction-free Zener limit v_Z, providing a clue to the apparent single-particle ILLT puzzle [11]. Even though the ME scenario can hardly be distinguished from ILLT according to the breakdown threshold in 2DEGs, it does explain the superpoissonian noise as a mere consequence of its collective nature. Note that the ME instability has also been considered to interpret quantum Hall fluid flows across an ionized impurity in Ref. [16] and DC magnetoresistance resonances in monolayer graphene (MLG) in Ref. [17].

The present work extends the noise investigation to MLG, which sustains a qualitatively different PHES due to its relativistic Landau level ladder, and a more pronounced effect of interactions on the ME branches of the PHES, as explained in Ref. [5]. This peculiarity of MLG is revisited below, and in Sec. III of the Supplemental Material, with new RPA calculations of the spectral function and magneto-optical conductivity σ_{MO}, accounting for screening by both hBN encapsulation and local back gating. Noise measurements, performed in high-mobility hBN-encapsulated graphene transistors, present a magnetic field and doping independent breakdown velocity $v_{bd}^{MLG} \simeq 1.4\ 10^5$ m/s at variance with massive BLG where $v_{bd}^{BLG} \propto \sqrt{B}$. Calculations of the PHES for our transistor geometry indicate that this constant breakdown velocity is actually determined by an empirical but universal impedance matching criterion: $\sigma_{MO} \sim 10^{-2} NG_K$, where NG_K is the Hall conductance. This small $\sigma_{MO}/NG_K \sim 10^{-2}$ ratio in QHE is reminiscent of the fine-structure constant $\alpha = Z_0 G_K$ governing light-matter coupling ruled by vacuum impedance $Z_0 = 377\ \Omega$. We conclude the paper by a comparison between MLG and BLG breakdown velocities at large doping, illustrating this qualitative difference between massive and massless ME instability supported by RPA theory.

II. MAGNETOTRANSPORT AND MICROWAVE NOISE MEASUREMENTS

The samples analyzed in this experiment have been previously used in the investigations of the Schwinger effect in Ref. [18] and/or flicker noise in Ref. [19]; they are described in the Supplemental Material [20] (Table. SM1). The transistors are embedded in coplanar wave guides for DC and microwave noise characterization at 4 Kelvin [see measurement setup in Fig. 1(a)]. The experiment is performed in the microwave frequency range to overcome flicker noise, which dominates up to the low-GHz range at large currents [19], and to access the QHEBD shot noise of interest. Data presented below concentrate on the hBN-encapsulated, bottom-gated, graphene sample AuS2 ($L \times W \times t_{hBN} = 16 \times 10.6 \times 0.032$ µm) which is described in Fig. 1 and in Ref. [18]. Graphene conductance is calculated after correcting for the (small) contact resistance effect. Low-bias magnetoconductance $G(V_g, B) = \partial I/\partial V$ [Fig. 1(b)], and the $\partial G/\partial V_g(V_g, B)$ fan chart [Fig. 1(c)], show clear MLG quantization down to low fields, i.e., for $B \gtrsim 0.5$ T in

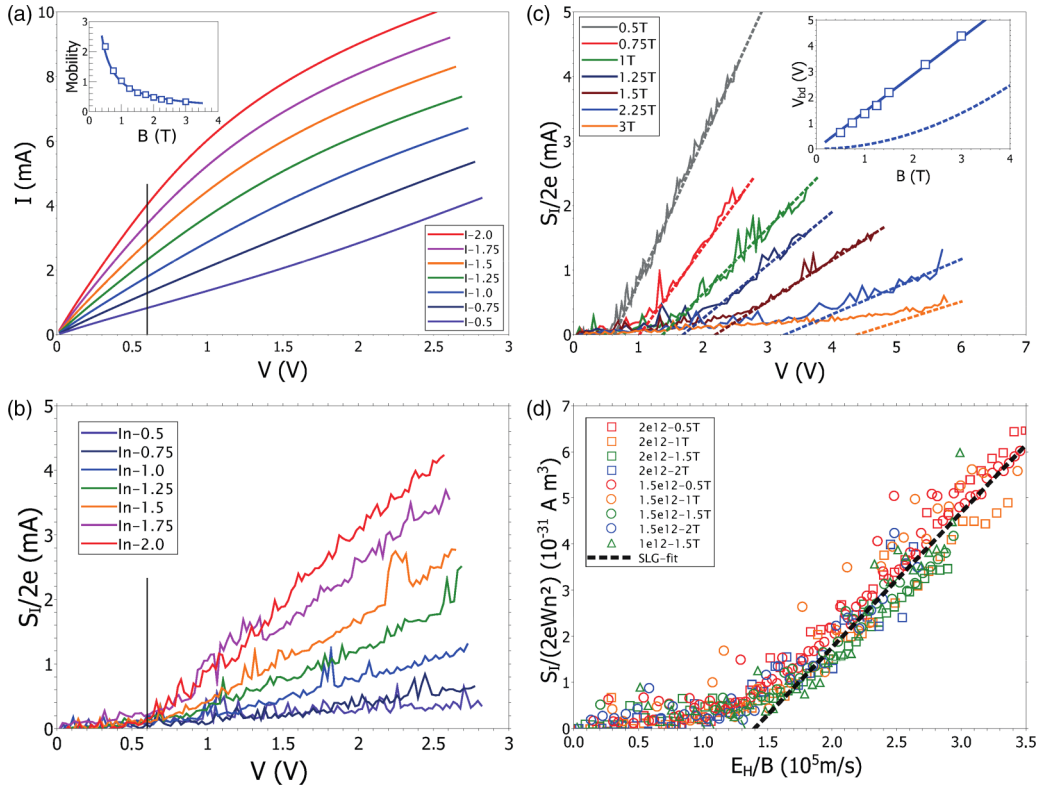

FIG. 2. MLG magnetotransport and noise scaling in sample AuS2. (a) High-bias transport current $I(V)$ at $B = 0.5$ T for $n = 0.5$–2.10^{12} cm^{-2} deviate from quantum Hall current $I = neV/B$ at the breakdown voltage $V_{bd} \simeq 0.6$ V (black line). Inset shows the measured low-bias mobility I/neV (squares, in m^2/Vs) and the $1/B$ Hall line. (b) Noise current $I_N(V) = S_I/2e$ at the same magnetic field and doping sequence, showing the onset of a large breakdown noise at the same V_{bd}, above a low noise quantum Hall background $I_N/V \simeq 0.1$ mS due to contact noise. (c) Voltage dependence of $I_N(V) = S_I/2e$ for various magnetic fields, at large doping $n = 2.10^{12}$ cm^{-2}. Inset shows the linear dependence $V_{bd}(B)$ corresponding to $v_{bd} = 0.14v_F$ (solid line), which strongly exceeds the Zener velocity (dashed line) at low field. (d) Scaling of breakdown noise with Hall velocity E_H/B for $n = 1$–2.10^{12} cm^{-2} and $B = 0.5$–2 T corresponding to $V_{bd} = 0.6$–2.4 V. It is represented by the master line $I_N/W = \gamma n^2[E_H/Bv_{bd} - 1]$ (dashed line), with $v_{bd}(n, B) = 1.4\ 10^5$ m/s (solid line), and $\gamma = 4.10^{-31}$ Am^3 corresponding to large breakdown noise currents $I_N/W \sim 40$ A/m (at $n = 1.10^{12}$ cm^{-2}).

accordance with the large $\mu \simeq 32$ m^2/Vs mobility. The specific MLG quantization, with plateaus at $\nu = 2(2N + 1)$, is clearly observed; the tiny width of the plateaus in Fig. 1(b) signals the absence of disorder-induced localized bulk states, which warrants the absence of electrostatic disorder. Plateaus gate voltages allow for the calibration of the gate capacitance at $C_g = 1$ mF/m^2 for a thickness of the bottom-hBN $t_{hBN} = 32$ nm with $\epsilon_{hBN} = 3.4$ [21]. The large biases entail prominent drain-gating effects, eventually leading to a pinchoff, as reported in Ref. [18] including for AuS2. This effect is compensated here by following the gating procedure described in Ref. [22] and routinely used in Refs. [11,18,19,23]; it consists of applying a bias-dependent gate voltage $V_g(V) = V_g(0) + \beta V$, $\beta \sim 0.4$ being adjusted to keep the resistance maximum at charge neutrality independent of bias at zero magnetic field. Figure 1(d) shows typical microwave $S_I(f)$ shot-noise spectra in increasing bias. Noise is expressed below in terms of the noise current $I_N = S_I/2e$ for an easy comparison with the DC transport current.

The high-bias magnetotransport and noise characteristics of sample AuS2 are described in Fig. 2. The current voltage relation $I(V)$, measured at $B = 0.5$ T in Fig. 2(a), shows a smooth crossover between the quantum Hall regime where $I \simeq I_H = \nu G_K V$ (inset) and the extremely high-bias metallic-like regime where the differential conductance recovers its zero-field value, which is set by the Zener-Klein conductivity [11,22]. The breakdown voltage $V_{bd} \approx 0.6$ V (black line) appears as a gradual deviation from the $I_H(V)$ Hall regime. By contrast, the current-noise characteristics $I_N(V)$, measured in the same conditions in Fig. 2(b), clearly distinguish two regimes: a quasinoiseless quantum Hall regime for $V \leqslant V_{bd} = 0.6$V, characterized by a residual contact noise conductance $I_N/V \sim 0.1$ mS, and a large differential noise conductance $G_N(n) = \partial I_N/\partial V \gtrsim 1$ mS for $V \geqslant V_{bd}$. The intersection between the two lines provides an unambiguous determination of the breakdown voltage V_{bd} which agrees with the transport determination in Fig. 2(a). In both $I(V)$ and $I_N(V)$, the breakdown voltage is found to be nearly doping independent, as opposed to the high-bias noise conductance $G_N \propto n^2$ in Fig. 2(b). Figure 2(c) shows the current noise $I_N(V)$ for different magnetic fields at a fixed large doping $n = 2.10^{12}$ cm^{-2}. It highlights the strong dependence of both $V_{bd} \propto B$ (inset) and $G_N \propto G_H \propto 1/B$, leading to a field-independent zero-bias extrapolate (not shown in the figure). These doping and field dependencies can be cast into the scaling displayed in Fig. 2(d), where noise data, collected over a broad $[n, B]$

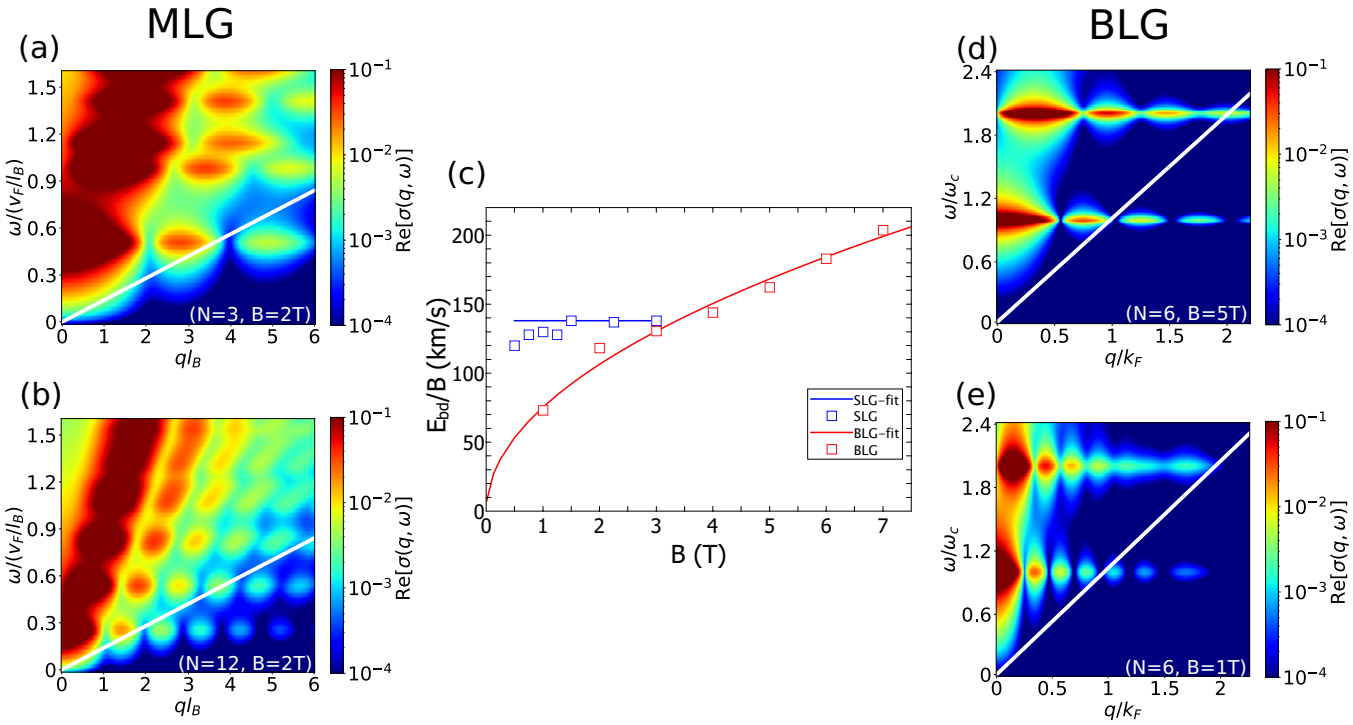

FIG. 3. Effect of gate and dielectric screening on the velocity-induced magnetoexciton (ME) instability in MLG and BLG. RPA magneto-optical conductivity spectra $\sigma_{MO}(q,\omega)$ (in units of NG_K) are plotted for the AuS2 MLG-sample geometry at $B = 2$ T for $N = 3$ in (a) and $N = 12$ in (b), and a similar BLG sample at $N = 6$ for $B = 5$ T in (d) and $B = 1$ T in (e). White lines correspond to the Doppler shifted drifting-electron spectrum for $v_{bd}^{MLG} = 0.14v_F$ in (a) and (b) and $v_{bd}^{BLG} = \hbar/m^* l_B\sqrt{N} \propto \sqrt{B}$ in (d) and (e). They separate the high-conductivity domain $\sigma_{MO} \gtrsim 10^{-2}\ NG_K$ from the low-conductivity one. (c) Experimental data of v_{bd}^{MLG} (blue squares) and v_{bd}^{BLG} (red squares from Ref. [11]), measured at the same $n = 2.10^{12}$ cm^{-2}, support these scalings and illustrate the main difference between MLG and BLG.

range, are found to collapse on the universal master line

$$\frac{I_N}{W} = \gamma n^2\left[\frac{E}{Bv_{bd}} - 1\right], \tag{1}$$

where $E = V/W$, $\gamma = 40 \times 10^{-32}\,\mathrm{Am}^3$, and $v_{bd} = 1.4 \times 10^5$ m/s. While the scaling differs from that of BLG [11], the noise amplitudes are comparable, with $I_N/W = 40$ A/m for $V = 2\,V_{bd}$ at $n = 10^{12}$ cm^{-2}. This noise scaling, with a doping-independent v_{bd}, contrasts with the doping-dependent ILLT breakdown threshold [dashed line in the inset of Fig. 2(c)]. Besides, the current noise density $S_I \propto n^2$ corresponds to a doping-independent velocity noise $S_v \propto S_I/n^2$, suggesting a kinematic interpretation of breakdown such as that provided by the ME instability, which. together with the constant breakdown velocity, justifies the scaling in Fig. 2(d).

III. A MAGNETO-OPTICAL CONDUCTIVITY CRITERION FOR QUANTUM HALL BREAKDOWN

To base this qualitative interpretation on a more quantitative analysis, we recalculate below the MLG-PHES of Ref. [5], adapting it for geometry and material parameters that are suitable for our experimental conditions. Figures 3(a) and 3(b) show the PHESs calculated in the RPA approximation of Ref. [5], where the spectral function Π^{RPA} with interactions is obtained from the bare spectral function Π^0 by the relation $\Pi^{RPA}(q,\omega) = \frac{\Pi^0(q,\omega)}{1-v(q,\omega)\Pi^0(q,\omega)}$.

Following the geometry of the AuS2 sample, we consider for the RPA approximation a screened 2D Coulomb potential $v(q,\omega)$ accounting for the hBN encapsulation and the presence of a local bottom gate. In this respect, we compute the electrostatic interaction within a vertical heterostructure composed of a graphene sheet, a top hBN layer of thickness d_2, and a bottom hBN layer of thickness d_1 (see values in Table SI1 of the Supplemental Material). The whole structure is placed on top of a Au backgate located at $z = 0$, with the half-space $z > (d_1 + d_2)$ filled with air, and hBN slabs are associated to frequency-dependent dielectric functions $\epsilon_x(\omega)$ and $\epsilon_z(\omega)$ for in-plane and out-of-plane components respectively. A schematic is presented in Fig. SI4.

In a similar manner to Ref. [24], and in accordance with the unscreened limit when $d_1 \to \infty$, we obtain the following expression for the potential:

$$v(q,\omega) = \frac{4\pi e^2 \sinh\left[d_1\sqrt{\frac{\epsilon_x}{\epsilon_z}}q\right]\left(\sqrt{\frac{\epsilon_x}{\epsilon_z}}q\epsilon_z \cosh\left[d_2\sqrt{\frac{\epsilon_x}{\epsilon_z}}q\right] + q\sinh\left[d_2\sqrt{\frac{\epsilon_x}{\epsilon_z}}q\right]\right)}{\sqrt{\frac{\epsilon_x}{\epsilon_z}}q\epsilon_z\left(\sqrt{\frac{\epsilon_x}{\epsilon_z}}q\epsilon_z \cosh\left[(d_1+d_2)\sqrt{\frac{\epsilon_x}{\epsilon_z}}q\right] + q\sinh\left[(d_1+d_2)\sqrt{\frac{\epsilon_x}{\epsilon_z}}q\right]\right)}, \tag{2}$$

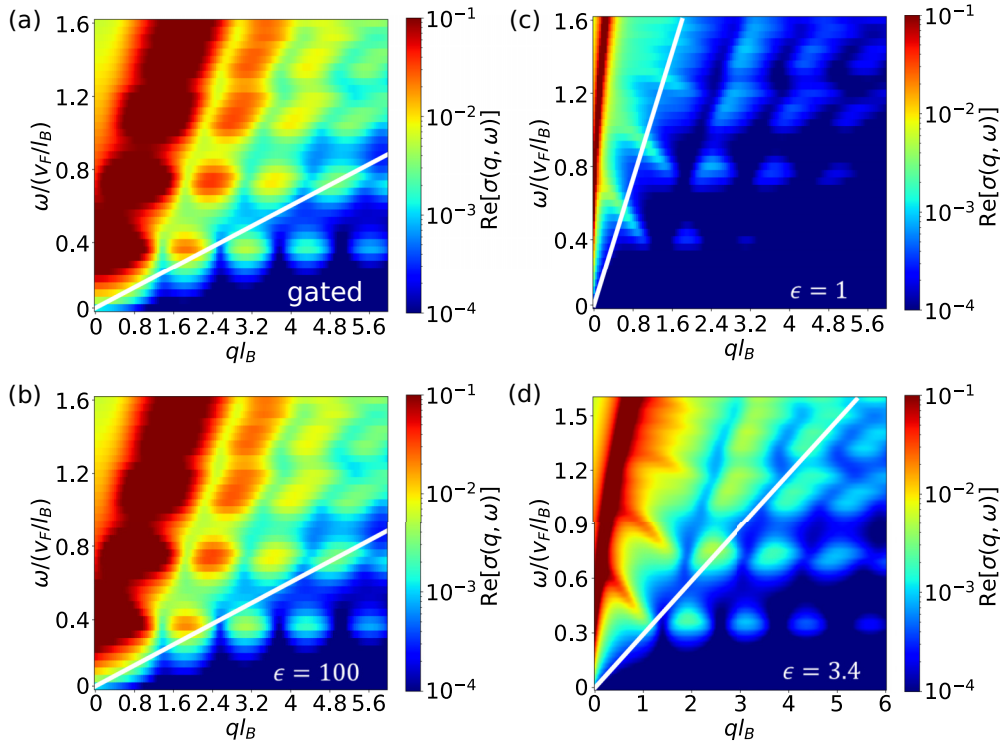

FIG. 4. RPA calculations of the MLG magneto-optical conductivity σ_{MO} for $N = 7$ and $B = 2$ T, and role of gate screening and interactions. The conductivity values are represented in units of the Hall conductance NG_K. Panel (a) shows the case of hBN encapsulation with an Au gate mimicking the AuS2 device (Eq. (2), with $d_1 = 32$ nm, $d_2 = 60$ nm, and dielectric functions for hBN ϵ_x and ϵ_z described in Ref. [24]). The conductivity PHES is very similar to that of an interactionless [$\epsilon_b = 100$ for an unscreened 2D Coulomb potential $v(q) = \frac{2\pi e^2}{\epsilon_b q}$] ungated sample shown in panel (b). Panels (c) and (d) focus on the role of interactions in the ungated case ($v(q) = \frac{2\pi e^2}{\epsilon_b q}$, with $\epsilon_b = 1$ [panel (c)] and $\epsilon_b = 3.4$ [panel (d)]). The white line in panels (a) and (b) correspond to the measured breakdown velocity for the AuS2 device $\omega = v_{bd}q$ with $v_{bd} = 0.14v_F$. The lines in panels (c) and (d) correspond to higher breakdown velocities following the discussion in the text. In all cases, the breakdown Doppler line separates the high-conductivity and low-conductivity PHES sectors at $\sigma_{MO} \sim 10^{-2}\, NG_K$.

where the ω dependence appears through the dielectric properties ϵ_x and ϵ_z of the hBN encapsulant. The low-q development of this full potential expression (see the SM) coincides to leading order with the potential $v_{\rm scr}(q) = (2\pi e^2/\epsilon_z q)[1 - \exp(-2d_1 q)] \sim 4\pi e^2 d_1/\epsilon_z$ of an electric point charge in the presence of a metallic gate at a distance d_1 from the graphene sheet, embedded in a dielectric environment described by the dielectric constant ϵ_z.

In the context of velocity-induced instability, we have plotted the magneto-optical conductivity spectrum $\Re[\sigma_{MO}(q,\omega)]$ (denoted σ_{MO} below), which is deduced from the usual spectral function $\Im[\Pi^{RPA}(q,\omega)]$ using the $\Re[\sigma_{MO}(q,\omega)] = -\frac{\omega e^2}{q^2}\Im[\Pi^{RPA}(q,\omega)]$ relation. Note that σ_{MO} suffers from nonphysical divergence in the low-q PHES limit, blurring the magnetoplasmon branch and hiding the existence of a spectral gap that appears more clearly in the spectral function (see Π^{RPA} spectra in Fig. SI5 of the Supplemental Material). This N-dependent bandgap is equal to the MLG cyclotron gap $\omega_c^{MLG} = (\sqrt{N+1} - \sqrt{N})v_F/l_B \simeq v_F/R_c$ (with R_c the cyclotron radius), similarly to BLG in Figs. 3(d) and 3(e), where $\omega_c^{BLG} = 1/m^* l_B^2$ is N independent (see the spectral function in Fig. SI7). Conductivity spectra are plotted for $N = 3$ [panel (a)] and $N = 12$ [panel (b)], displayed in logarithmic scale to map their steep ω and q dependencies, and normalized to the Hall conductivity NG_K (per spin and valley) for a direct comparison of electronic and collective electron-hole excitation's conductivity. The momentum and energy scales are expressed in MLG-relevant dimensionless units ql_B and $\omega l_B/v_F$, which imply a magnetic-field independence of the ME branches phase velocity $v_{ME} = \omega_{ME}/q$. Remarkably, the ME optical conductivity σ_{MO} is steeply increasing with v_{ME}, with $\sigma_{MO} \sim (3.10^{-4}$–$3.10^{-2})\, NG_K$ for $v_{ME} = (0.06$–$0.35)\, v_F$.

The effect of screening is quite substantial in MLG, as depicted in Fig. 4 and in the SM, and much more prominent than in BLG (Fig. SI8), especially at large q. The white lines in Figs. 3(a) and 3(b) correspond to the Doppler-shifted electronic energy $\omega = v_{bd}q$ of drifting electrons, calculated at the measured breakdown velocity $v_{bd} = 0.14v_F$ of Fig. 2. In both the $N = 3$ [panel (a)] and the $N = 12$ [panel (b)] examples, this line separates a high ME-conductivity domain for $\omega \gtrsim v_{bd}q$, where $\sigma_{MO} \gtrsim 10^{-2} NG_K$, from a low conductivity domain for $\omega \lesssim v_{bd}q$; the $N = 7$ example displayed in Figure 4 a shows similar behavior. The observation of an N and B independent ME instability, at a velocity $v_{BD} \simeq v_{ME} = $ cst. controlled by a fixed $\sigma_{MO} \sim 10^{-2} NG_K$ constraint, is consistent with a collective wave interpretation, even if the precise value of the optical impedance threshold remains to be established theoretically. It is obviously consistent with our experimental observation in Fig. 2 of an N- and B-independent breakdown velocity, a feature observed in all tested Au-gated samples (see Table SI1 in the Supplemental Material). Unlike in BLG, the $v_{bd} = $ cst. breakdown velocity of MLG, inferred

from the above conductivity criterion, exceeds the ILLT $v_Z \propto \sqrt{B}$, especially at low B.

Let us recall that the situation is different in BLG. Figures 3(d) and 3(e) reproduce the theoretical analysis for a similar BLG sample, such as that measured in Ref. [11]; in this case, we rely on the calculations for a conventional 2DEG, that match the bilayer case in the large N limit [4]. The energy (ω/ω_c) and momentum (q/k_F) reduced units are adapted for a massive 2DEG-like BLG, but the reduced conductivity scale σ_{MO}/NG_K is the same. The two panels correspond to the same $N = 6$, but different magnetic fields $B = 5$ T [panel (d)] and $B = 1$ T [panel (e)]. Contrarily to MLG, the phase velocity ω_{ME}/q is not magnetic-field independent in this representation, as $\omega_c \propto B$ and $k_F \propto 1/l_B \propto \sqrt{B}$ have different B dependencies. As a consequence, positioning an identical Doppler line on the two reduced-unit plots amounts to taking a $v_{bd} \propto \sqrt{B}$. Figs. 3(d) and 3(e) show that this criterion also corresponds to a consistent $\sigma_{MO} \sim 10^{-2} NG_K$ criterion for the ME instability, which is met in BLG at (q, ω)-localized ME conductivity peaks. This optical impedance analysis shows that for BLG, and more generally 2DEGs, the ME instability and Zener ILLT, which are basically different, give consistent and similar breakdown velocities in BLG, confirming earlier statements of Ref. [11]. Finally, Fig. 3(c) illustrates the qualitative difference between MLG and BLG in a plot of $v_{bd}(B)$ at a large $n = 2.10^{12}$ cm^{-2} (BLG data are reproduced from Fig. 2 of Ref. [11]), with $v_{ME}^{MLG} \simeq 0.14 v_F$ (blue line) and $v_{ME}^{BLG} = \hbar/m^* l_B \sqrt{N} \propto \sqrt{B}$ (red line for $N = 5$) [11]. Let us note that the magnetic field dependencies $v_{bd}^{MLG} = \text{cst.}$ and $v_{bd}^{BLG} \propto \sqrt{B}$ merely reflect the energy dependence of the Fermi velocity, $v_F^{MLG}(\varepsilon_L) = \text{cst.}$ and $v_F^{BLG}(\varepsilon_L) \propto \sqrt{\varepsilon_L}$, when taken at the Landau energy $\varepsilon_L = \hbar\omega_c \propto B$. Therefore, the breakdown velocity reflects the relativistic character of transport in graphene.

IV. INFLUENCE OF COULOMB INTERACTIONS ON BREAKDOWN VELOCITY

Relying on the good mapping of the ME-scenario with experiment, we exploit the RPA calculations further in Fig. 4 and Secs. III B and III C of the Supplemental Material to model breakdown in varied graphene geometries such as graphene in vacuum [with an unscreened 2D Coulomb potential $v(q) = \frac{2\pi e^2}{\epsilon_b q}$ where $\epsilon_b = 1$] or semi-infinite hBN embedding ($\epsilon_b = 3.4$), keeping a systematic benchmark of MLG and BLG cases, and assuming the existence of a universal impedance-matching condition. For MLG, we show in Figs. 4(a) and 4(b) that screening by the bottom gate in AuS2 [panel (a)] is equivalent to a semi-infinite, $\epsilon_b = 100$ dielectric [panel (b)], meaning that both PHESs correspond to the fully screened conductivity: the presence of a close local gate, that restricts the Coulombian interaction at shorter range, restores the magneto-optical conductivity spectrum observed in the non-interacting case. Effect of interactions, which is maximal for ungated suspended graphene [$\epsilon_b = 1$ in panel (c)], amounts to suppressing the conductivity amplitude below the $\sigma_{MO} \sim 10^{-2} NG_K$ ME-instability threshold over most of the ME spectrum leading to an enhanced breakdown velocity $v_{bd} \simeq 0.5 v_F$ (white line). Given the impedance matching condition $\sigma_{MO} \sim 10^{-2} NG_K$, we conclude that the ME-instability velocity of MLG is a constant, in the range $v_{ME} = [0.14, 0.5]\, v_F$ that depends on screening. The same analysis is performed for BLG in Fig. SI8, showing that the large-q PHES sector is, to a large extent, insensitive to screening, yielding a Zener-like breakdown velocity $v_{ME}^{BLG} = \frac{\hbar}{m^* R_c}$.

V. CONCLUSION

In conclusion, we have shown that bulk quantum Hall breakdown is controlled by the magnetoexciton instability in both MLG and BLG with a threshold $v_{\text{drift}} \geqslant v_{ME}$. More precisely, instability is defined by a universal conductivity criterion $\sigma_{MO} \sim 10^{-2} NG_K$. This universal criterion explains the qualitative differences between the massless MLG and massive BLG. Whereas the BLG-ME instability mimics single-particle ILLT, that of MLG is sensitive to screening by the embedding dielectric and local gates. Screening reduces the breakdown velocity, and gated transistors correspond to the fully screened regime. Both studies promote shot noise as a sensitive probe of quantum Hall transport, RPA as a relevant theoretical tool to tackle interactions and screening, and high-velocity transport as a sensitive probe of the large-momentum collective excitations, as suggested by Landau [25]. Understanding the combined effects of Landau quantization and interactions in the collective modes of the integer quantum Hall effect is a prerequisite before addressing the more challenging case of the fractional regime, where elusive magnetorotons may come into play. Finally, and on a broader scope, let us mention that the magnetoexciton instability is a quantum-Hall-matter light coupling effect, which belongs to a domain of current interest, including the recent evidence of the effect of cavity vacuum fields on integer quantum Hall transport [26].

Data are available on a public Zenodo repository in Ref. [27].

ACKNOWLEDGMENTS

A.S. thanks Prof. C. R. Dean for hospitality and introducing him to the fabrication of high-quality graphene-hBN heterostructures. The research leading to these results has received partial funding from the European Union Horizon 2020 research and innovation program under Grant Agreement No. 881603 "Graphene Core 3," and from the French ANR-21-CE24-0025-01 "ELuSeM."

A.S., B.P., and E.B. conceived the experiment. A.S. conducted device fabrication and measurements under the guidance of M.R. in the early developments. T.T. and K.W. have provided the hBN crystals. A.S., M.O.G., and B.P. developed the models and theoretical interpretations. A.S., G.F., J.M.B., G.M., C.V., B.P., and E.B. participated to the data analysis. B.P. wrote the manuscript with assistance of A.S. and E.B., and contributions from the coauthors.

The authors have no conflict of interest to disclose.

[1] K. von Klitzing, G. Dorda, and M. Pepper, New Method for High-Accuracy Determination of the Fine-Structure Constant Based on Quantized Hall Resistance, Phys. Rev. Lett. **45**, 494 (1980).

[2] A. Tzalenchuk, S. Lara-Avila, A. Kalaboukhov, S. Paolillo, M. Syvajarvi, R. Yakimova, O. Kazakova, T. J. B. M. Janssen, V. Fal'ko, and S. Kubatkin, Towards a quantum resistance standard based on epitaxial graphene, Nat. Nanotech. **5**, 186 (2010).

[3] R. Ribeiro-Palau, F. Lafont, J. Brun-Picard, D. Kazazis, A. Michon, F. Cheynis, O. Couturaud, C. Consejo, B. Jouault, W. Poirier, and F. Schopfer, Quantum Hall resistance standard in graphene devices under relaxed experimental conditions, Nat. Nanotech. **10**, 965 (2015).

[4] M. O. Goerbig, Electronic properties of graphene in a strong magnetic field, Rev. Mod. Phys. **83**, 1193 (2011).

[5] R. Roldán, J.-N. Fuchs, and M. O. Goerbig, Collective modes of doped graphene and a standard two-dimensional electron gas in a strong magnetic field: Linear magnetoplasmons versus magnetoexcitons, Phys. Rev. B **80**, 085408 (2009).

[6] S. M. Girvin, A. H. MacDonald, and P. M. Platzman, Magneto-roton theory of collective excitations in the fractional quantum Hall effect, Phys. Rev. B **33**, 2481 (1986).

[7] T. Jolicoeur, Shape of the magnetoroton at $\nu = 1/3$ and $\nu = 7/3$ in real samples, Phys. Rev. B **95**, 075201 (2017).

[8] P. Streda and K. von Klitzing, Critical non-dissipative current of the quantum Hall regime., J. Phys. C: Solid State Phys. **17**, L483 (1984).

[9] K. Panos, R. R. Gerhardts, J. Weis, and K. von Klitzing, Current distribution and Hall potential landscape towards breakdown of the quantum Hall effect: A scanning force microscopy investigation, New J. Phys. **16**, 113071 (2014).

[10] L. Eaves and F. W. Sheard, Size-dependent quantised breakdown of the dissipationless quantum Hall effect in narrow channels, Semicond. Sci. Technol. **1**, 346 (1986).

[11] W. Yang, H. Graef, X. Lu, G. Zhang, T. Taniguchi, K. Watanabe, A. Bachtold, E. H. T. Teo, E. Baudin, E. Bocquillon, G. Fève, J. M. Berroir, D. Carpentier, M. O. Goerbig, and B. Plaçais, Landau Velocity for Collective Quantum Hall Breakdown in Bilayer Graphene, Phys. Rev. Lett. **121**, 136804 (2018).

[12] C. Chaubet and F. Geniet, Nonequilibrium occupation of Landau levels and universal critical field in the quantum-Hall-effect breakdown, Phys. Rev. B **58**, 13015 (1998).

[13] I. A. Dmitriev, A. D. Mirlin, D. G. Polyakov, and M. A. Zudov, Nonequilibrium phenomena in high Landau levels, Rev. Mod. Phys. **84**, 1709 (2012).

[14] L. Bliek, E. Braun, G. Hein, V. Kose, J. Niemeyer, G. Weimann, and W. Schlapp, Critical current density for the dissipationless quantum Hall effect, Semicond. Sci. Technol. **1**, 110 (1986).

[15] K. Chida, T. Hata, T. Arakawa, S. Matsuo, Y. Nishihara, T. Tanaka, T. Ono, and K. Kobayashi, Avalanche electron bunching in a Corbino disk in the quantum Hall effect breakdown regime, Phys. Rev. B **89**, 235318 (2014).

[16] A. M. Martin, K. A. Benedict, F. W. Sheard, and L. Eaves, Model for the Voltage Steps in the Breakdown of the Integer Quantum Hall Effect, Phys. Rev. Lett. **91**, 126803 (2003).

[17] M. T. Greenaway, P. Kumaravadivel, J. Wengraf, L. A. Ponomarenko, A. I. Berdyugin, J. Li, J. H. Edgar, R. K. Kumar, A. K. Geim, and L. Eaves, Graphene's non-equilibrium fermions reveal Doppler-shifted magnetophonon resonances accompanied by Mach supersonic and Landau velocity effects, Nat. Commun. **12**, 6392 (2021).

[18] A. Schmitt, P. Vallet, D. Mele, M. Rosticher, T. Taniguchi, K. Watanabe, E. Bocquillon, G. Fève, J. M. Berroir, C. Voisin, J. Cayssol, M. O. Goerbig, J. Troost, E. Baudin, and B. Plaçais, Mesoscopic Klein-Schwinger effect in graphene, Nat. Phys. **19**, 830 (2023).

[19] A. Schmitt, D. Mele, M. Rosticher, T. Taniguchi, K. Watanabe, C. Maestre, C. Journet, V. Garnier, G. Fève, J. M. Berroir, C. Voisin, B. Plaçais, and E. Baudin, High-field 1/f noise in hBN-encapsulated graphene transistors, Phys. Rev. B **107**, L161104 (2023).

[20] See Supplemental Material at http://link.aps.org/supplemental/10.1103/PhysRevB.108.085438 for a complete description of the device series and a detailed presentation of the PHES calculations introduced in the text.

[21] A. Pierret, D. Mele, H. Graef, J. Palomo, T. Taniguchi, K. Watanabe, Y. Li, B. Toury, C. Journet, P. Steyer, V. Garnier, A. Loiseau, J.-M. Berroir, E. Bocquillon, G. Fève, C. Voisin, E. Baudin, M. Rosticher, and B. Plaçais, Dielectric permittivity, conductivity and breakdown field of hexagonal boron nitride, Mater. Res. Express **9**, 065901 (2022)

[22] W. Yang, S. Berthou, X. Lu, Q. Wilmart, A. Denis, M. Rosticher, T. Taniguchi, K. Watanabe, G. Fève, J.-M. Berroir, G. Zhang, C. Voisin, E. Baudin, and B. Plaçais, A graphene Zener-Klein transistor cooled by a hyperbolic substrate, Nat. Nanotech. **13**, 47 (2018).

[23] E. Baudin, C. Voisin, and B. Plaçais, Hyperbolic phonon polariton electroluminescence as an electronic cooling pathway, Adv. Funct. Mater. **30**, 1904783 (2020).

[24] A. Principi, M. B. Lundeberg, N. C. H. Hesp, K.-J. Tielrooij, F. H. L. Koppens, and M. Polini, Super-Planckian Electron Cooling in a van der Waals Stack, Phys. Rev. Lett. **118**, 126804 (2017).

[25] L. Landau, Theory of the superfluidity of helium II, Phys. Rev. **60**, 356 (1941).

[26] F. Appugliese, J. Enkner, G. L. Paravicini-Bagliani, M. Beck, C. Reichl, W. Wegscheider, G. Scalari, C. Ciuti, and J. Faist, Breakdown of topological protection by cavity vacuum fields in the integer quantum Hall effect, Science **375**, 1030 (2022).

[27] https://doi.org/10.5281/zenodo.7814596.